Aerodynamic Performance of a Tip-Mounted Propeller-Wing System at Positive and Negative Thrust

Sinnige, T.; Corte, B. Della

DOI
10.2514/6.2024-3520

Publication date
2024

Document Version
Final published version

Published in
AIAA Aviation Forum and ASCEND, 2024

AIAA Aviation Forum and ASCEND co-located Conference Proceedings
29 July - 2 August 2024, Las Vegas, Nevada
AIAA AVIATION FORUM AND ASCEND 2024
10.2514/6.2024-3520

Aerodynamic Performance of a Tip-Mounted Propeller-Wing System at Positive and Negative Thrust

T. Sinnige * and B. Della Corte †
Delft University of Technology, Delft, 2629 HS, Netherlands

A wind-tunnel experiment was performed at the DNW Low-Speed Tunnel with a powered propeller-wing model to prove the concept of energy-harvesting with propellers and assess its impact on the wing performance. By separating the contributions of the propeller and wing to the overall system forces, both for positive and negative thrust settings improved understanding was obtained of the propeller-wing interaction. A tip-mounted propeller configuration was simulated. At positive thrust settings, the operation of the propeller increased the lift gradient and improved the aerodynamic efficiency of the wing (L/D) by 10-35% compared to the propeller-off configuration. At $C_L = 0.5$ and net zero force in streamwise direction the benefit was 12%, while at $C_L = 1.0$ and a net force in streamwise direction of approximately three times the wing drag the benefit was 32%. At negative thrust, the propeller operation decreased the lift gradient, but the wing aerodynamic efficiency was still higher than that of the propeller-off configuration. This was an unexpected result, which was explained by the reduction in friction drag on the wing immersed in the propeller slipstream due to the lower dynamic pressure, and a possible reduction in wing induced drag due to downwash on the outboard part of the wing. The aileron effectiveness was decreased by about 10% when switching from positive to negative thrust operation. However, for angles of attack up to approximately 14 degrees even at negative thrust, the aileron effectiveness was still higher than for the clean wing.

I. Introduction

Wingtip-mounted propellers have been shown to enhance aerodynamic performance through a beneficial interaction between the propeller-induced flowfield and the wing. When operating the propeller in an inboard-up configuration, the upwash induced by the propeller decreases the local induced drag of the wing, thereby providing a potential performance gain compared to the unpowered configuration. The fundamental mechanisms behind this performance gain have been explained in previous work [1–5] and therefore will not be elaborated upon again here.

Although it is known that performance gains can be achieved, knowledge of the interactions is still incomplete. A major shortcoming of existing data sets is the lack of separation between wing and propeller loads. Not only is this required to better understand the source of the performance gains, but also for validation of numerical simulations of such configurations. Moreover, the change in the propeller-wing interaction when switching from positive to negative thrust mode has not been considered before in depth in the literature. The goal of the experiment described in this paper was to fill those two knowledge gaps.

The analysis of the data provides more accurate estimates of the expected aerodynamic performance gains of tip-mounted propellers than obtained before. Moreover, the change in wing loading and installed propeller loading due to operation of propellers at negative thrust is assessed for the first time. Finally, the data set is aimed to be of sufficient quality to serve as a reference validation case for development and benchmarking of numerical models.

II. Experimental Setup

Powered testing with a propeller-wing model was done at the DNW-LST wind tunnel. This chapter describes the details of the experimental setup.

A. Wind Tunnel

The wind-tunnel experiment was carried out at the Low-Speed Tunnel (LST) of the German-Dutch Wind tunnels (DNW). The LST is a closed-circuit, atmospheric wind-tunnel featuring a rectangular test section measuring 3.0 m

*Assistant Professor, Flow Physics and Technology Department, Faculty of Aerospace Engineering, AIAA Member.
†Postdoctoral researcher, Flow Physics and Technology Department, Faculty of Aerospace Engineering.

x 2.25 m. The wind tunnel is used for industrial aerodynamic testing of model components and half models. The turbulence levels in the tunnel are low. Turbulence induced by vorticity convected into the test section through the contraction amounts to about 0.02% in streamwise direction and 0.03% in in-plane directions on the tunnel center line for velocities up to 60 m/s (which includes 99% of the test program discussed in this paper). Turbulence induced by vorticity in the wall boundary layers is dominant near the tunnel walls.

B. Model Configurations

Three different model configurations were considered:

1) Nacelle-off;
2) Nacelle-on, blades-off;
3) Nacelle-on, blades-on.

Photographs of the 3 model configurations installed in the DNW-LST wind tunnel are provided in Fig. 1.

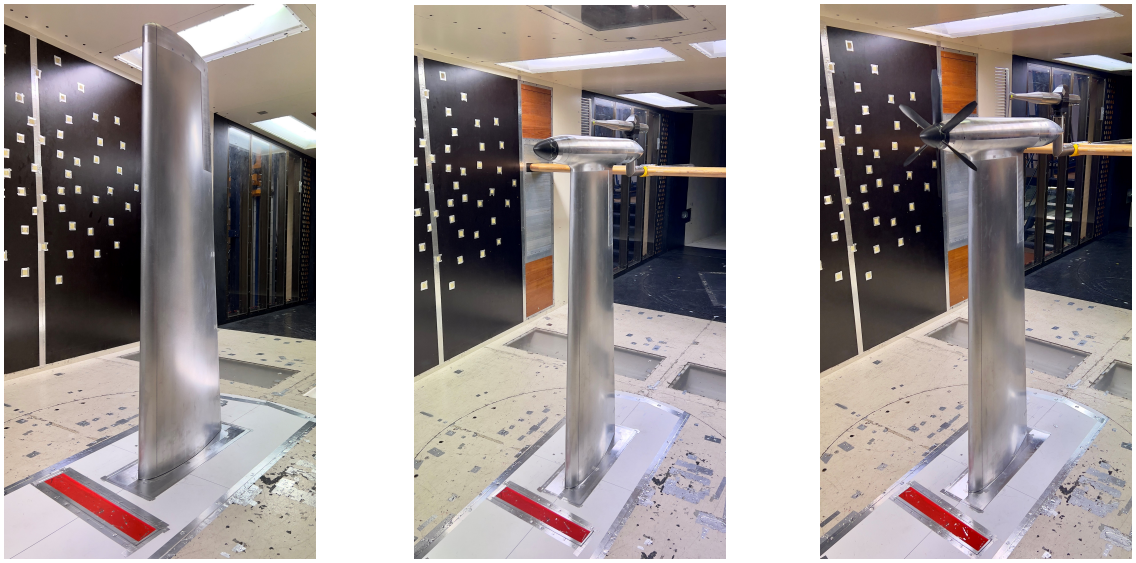

(a) Nacelle-off **(b) Nacelle-on, blades-off** **(c) Nacelle-on, blades-on**

Fig. 1 Photographs of wind-tunnel model installed in the DNW-LST wind tunnel.

C. Model Geometry and Features

The wing model consisted of a tapered, untwisted, straight wing, with an aspect and taper ratio of 6.8 and 0.7, respectively, and zero sweep angle at the quarter-chord line. A NASA MS-0317 airfoil section [6] is used along the entire span. Technical drawings of the model are reported in Fig. 2.

The span of the wing, from wind-tunnel floor to tip is 1628.6 mm, equal to approximately four times the propeller diameter, D. The span was sized such that the resulting clearance between the test-section ceiling and the propeller tip is equal to approximately one propeller diameter. This clearance was considered sufficient to minimize the wall-interference effects on the propeller performance, according to a previous study featuring a similar propeller geometry.

The wing chord distribution was designed such that the chord at the section corresponding to 70% of the propeller radius is equal to the propeller diameter. This resulted in a root chord of 559.6 mm and a tip chord of 391.7 mm.

The wing model is equipped with a 20%-chord plain aileron at the outboard section. The design of the aileron was adapted from that proposed by NASA for an airfoil of the same family [7]. Moreover, the wing features a modular tip that can be removed to install the nacelle (nacelle-on configuration).

The propeller model is the 6-bladed TU Delft XPROP propeller. The propeller is mounted on an axisymmetric nacelle which is installed with a 3.5 deg (tip down) offset angle with respect to the wing chord line. The installation angle was selected to align the propeller with the local flow direction in cruise conditions, corresponding to a wing lift coefficient of 0.50. The rotating parts (i.e. spinner, and propeller—hub assembly) are offset from the stationary parts through a 0.5 mm gap. Separate experiments were done with the uninstalled propeller to obtain reference performance data.

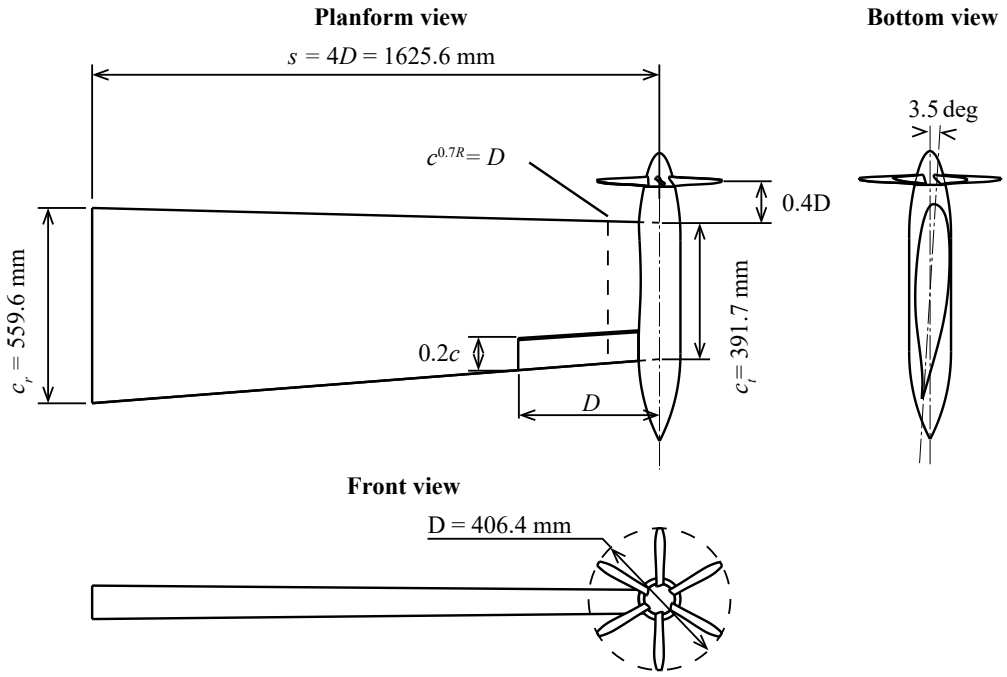

Fig. 2 Orthographic views of the wing model (propeller-on configuration).

The propeller is driven by a three-phase brushless electric outrunner motor, housed inside the nacelle. Electric power was provided by a bi-directional 15 kW power supply. The motor was controlled through an electronic speed controller. The nacelle was instrumented with an optical encoder to accurately measure the rotational speed of the propeller.

Turbulent transition was forced on both the wing and the nacelle surfaces through the application of carborundum strips. Carborundum Grit 60 was used (average particle diameter 250 microns, minimum 177 microns, maximum 390 microns) on both suction and pressure sides at approximately 12% of the chord. This position was chosen as a compromise between proximity to the leading edge and interference with the wing pressure taps and surface microphones.

D. Operating Conditions

Tests were performed at constant freestream Mach number and varying angle of attack, propeller advance ratio, aileron deflection angle, and wall blowing coefficient.

1. Freestream Mach number

For the nacelle-off configuration, freestream Mach numbers of 0.090, 0.120, 0.150, 0.175, and 0.200 were considered. For the nacelle-on configuration, tests were performed at freestream Mach numbers of 0.120 and 0.175, with only selected conditions evaluated at the Mach number of 0.175.

The largest part of the test program was performed at freestream Mach number of 0.120. Moreover, a large number of conditions was evaluated at M=0.175 especially for validation purposes. Measurements with blowing enabled were only taken at a freestream Mach number of 0.175.

2. Angle of attack

Different angle of attack ranges were used for the different model configurations and different freestream conditions. The maximum angle of attack considered was 22.5 deg for blade-off measurements at $M_\infty = 0.120$, and 15 deg for measurements at $M_\infty = 0.175$. The minimum angle of attack was 5 deg. For the prop-on test program, the maximum angle of attack was limited to 15 deg at all Mach numbers.

3. Propeller pitch settings and advance ratio

Two propeller pitch settings were considered: 30 and 45 degrees at $r/R = 0.7$. For each pitch setting, sweeps of advance ratios were performed to cover a significant range of thrust settings. For the 30 deg pitch setting, both positive and negative thrust settings were considered. The positive thrust settings correspond to the conventional propulsive mode, while the negative thrust settings correspond to the energy harvesting mode. The considered ranges of advance ratio $J = V_\infty/nD$ and associated thrust coefficients $T_C = T/(\rho_\infty V_\infty^2 D^2)$ were:

- 30 deg pitch
  - positive thrust domain $0.9 < J < 1.2$, $+0.05 < T_C < +0.35$ (approximately);
  - negative thrust domain $1.5 < J < 2.0$, $-0.09 < T_C < -0.03$ (approximately).
- 45 deg pitch
  - positive thrust domain $1.5 < J < 2.1$, $+0.03 < T_C < +0.15$ (approximately).

(n = propeller rotational speed [Hz]; D = prop diameter = 0.4064 m)

4. Aileron settings

The slipstream of the tip-mounted propeller directly affects the flow over the outboard aileron, thereby possibly affecting roll control performance. To be able to assess the change in roll control performance when changing from positive to negative thrust, measurements were performed at different aileron deflection angles. The main part of the test program was done at 0, +10, and −10 degrees of aileron deflection. Additionally, measurements were performed at +5 deg for selected conditions with the nacelle-off configuration. Deflection angles of +20, −5 and −20 degrees were also prepared, but not tested due to lack of time and higher-than-expected flow separation at the 10 deg deflection settings.

5. Wall blowing settings

The optimal blowing setting for the wall blowing system was tuned before the start of the main measurement campaign and expressed in terms of a nondimensional blowing coefficient, defined as the ratio of mass flow times velocity through the blowing slot with respect to freestream dynamic pressure times area of the blowing slot ($C_\mu = \dot{m}_{\text{bl}} V_{\text{bl}}/Q_\infty A_{\text{bl}}$). Once identified, this blowing coefficient was not further varied. Measurements were therefore taken with blowing off or on at fixed blowing coefficient of 30 (±1).

E. Measurement Techniques

1. Force and moment measurements

The time-averaged integral aerodynamic forces and moments acting on the entire model assembly were measured through an external six-component balance. The balance features a calibration uncertainty of 0.1% of the full-scale range on the drag and lift components, which amounts to approximately 2 N for both components.

The propeller performance was measured with an internal six-component rotating balance [8]. The uncertainty of this balance is within 0.05% of full-scale for thrust and 0.2% of full scale for torque. This amounts to approximately 0.2 N of thrust and 0.06 Nm for torque. Through this balance, the forces and moments acting on the propeller blades, hub and spinner were quantified.

The presence of the gap between the rotating and stationary parts was accounted in the internal balance measurements through the back-plate pressure correction. The pressure distribution on the front face of the stationary part of the nacelle was measured through 24 pressure taps. The taps were arranged in groups of 4 taps at 6 azimuthal angles. The integral pressure force acting on this surface was removed from the forces measured by the balance. In this way the pressure force acting on the back of the balance itself was not accounted for in the measurements.

The combination of the data from the external and internal balances allowed the separation of the forces acting on the propeller and on the wing only surfaces, giving insights into the installation effects on each sub-system and their mutual interactions.

2. Surface pressure measurements

The wing and nacelle models are instrumented with 594 and 55 static pressure taps, respectively. On the wing, the taps are organized in chordwise rows along 10 wing sections. The instrumented sections are distributed non-uniformly along the span, with a denser resolution in the portion of the wing washed by the propeller slipstream. At each station,

54 taps are distributed on both sides of the airfoil. The chordwise distribution was obtained by combining a cosine distribution for $0 < x/c \leq 0.30$ and a uniform distribution for $x/c > 0.30$.

Moreover, 61 MMaudio MM-PSM-L back electret condenser microphones are installed in the wing to assess the time-dependent pressure distribution on the model surface. The microphone sensors were installed in a recessed cavity communicating with the external surface through a hole measuring 0.4 mm in diameter.

3. Flowfield measurements

A rake of 18 five-hole probes was used to quantify the distribution of total pressure and velocity components in the wake of the model. The measurement plane was fixed at $1c = 1D$ downstream of the trailing edge of the wing at the section corresponding to the $0.7R$ propeller section. The rake features a 15 mm pitch between the probes and total width of 255 mm and it was mounted vertically, i.e. aligned with the spanwise direction. Figure 3 shows a photograph of the wake rake installed in the test section.

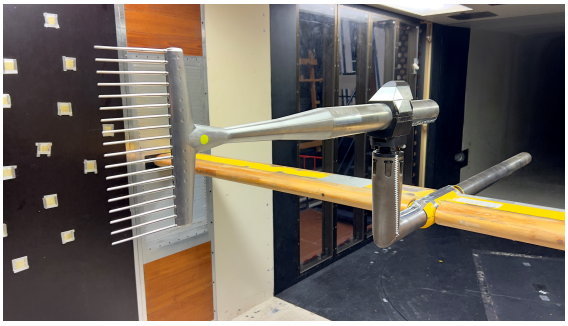

Fig. 3 Photograph of the wake survey measurement setup.

Wake rake measurements were taken for selected operating conditions. For each case, the wake rake was traversed in the lateral direction at a speed of 2.5 mm/s. Samples were averaged out over 1 s to obtain a single data point. These continuous lateral sweep were repeated 9 times for different spanwise positions of the wake rake to cover the entire wake. In total, the rake covered a region from 67% to 112% of the wing span. The spanwise displacement were staggered to achieve a final resolution of 5 mm in the spanwise direction. The lateral position of the wake rake was adjusted based on the wing incidence in order to ensure that the wing wake and propeller slipstream were captured in the measurement plane.

4. Tuft flow visualization

The surface flow on the model was visualized through the application of tufts on the nacelle and wing surfaces. Both the suction and pressure side of the model were observed simultaneously. Spanwise strips of tufts were taped to the surface with a uniform chordwise distribution. The resulting spacing was equal to approximately 50 mm in both the spanwise and chordwise direction. Dedicated measurements were carried out at selected operating conditions. These measurements provide qualitative flow visualization data that aid the understanding of the main flow phenomena (e.g. the occurrence of flow separation) and hence of the campaign results.

F. Data Analysis and Processing

1. Boundary corrections

The hard-walled test section provides an excellent environment for aerodynamic measurements. The data have been corrected for the following boundary effects:

- Blockage
  - Solid blockage wing
  - Solid blockage nacelle
  - Propeller slipstream blockage
  - Wake blockage

- Lift interference
  - Angle of attack correction
  - Drag correction
  - Pitching moment correction

The boundary corrections were performed live and wind-tunnel conditions were set based on corrected data, except for the angle of attack. The lift interference correction ignored the contribution from the propeller normal force to the model lift. This was assumed to be an acceptable simplification considering the low ratio of propeller normal-force induced lift to the wing lift.

The acoustic measurements will have been affected by acoustic reflections. The tonality of propeller noise will result in a complex interference pattern which affects the directivity of the measured noise emissions. No attempts were made to correct the acoustic data for reflections. Therefore, the propeller noise measurements were not intended as validation measurements, but rather as exploratory measurements to identify potential major shifts in dominant noise levels comparing the positive to the negative thrust regimes.

2. Response models wing performance propeller-off

Polynomial response models for the wing performance without propeller were generated for lift and drag coefficients with respect to angle of attack using the data from the external balance. A 3rd order polynomial was used to fit the lift coefficient. A 4th order polynomial was used to fit the drag coefficient. 95% nonsimultaneous confidence intervals were computed to quantify the accuracy of the response models. Figure 4 provides an example of the results for the case without nacelle, with tripping installed.

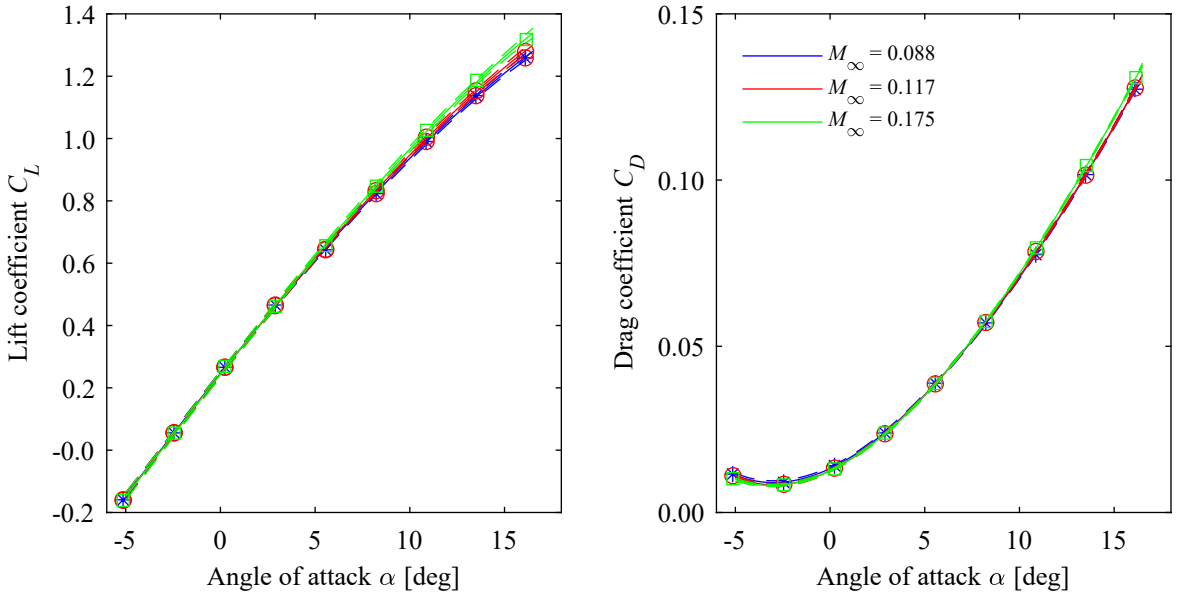

(a) Lift **(b) Drag**

Fig. 4 Example fitting results of response models for lift and drag coefficients (nacelle-off, roughness on).

3. Response models system performance propeller-on

Polynomial response models for the system performance with propeller were generated for the lift and drag coefficients with respect to angle of attack and advance ratio at fixed pitch using the data from the external balance. For the lift coefficient, the model was 3rd order in angle of attack and 3rd order in advance ratio, including all interaction terms. For the drag coefficient, the model was 4th order in angle of attack and 3rd order in advance ratio, including all interaction terms. For the measurements performed at a pitch setting of 30 deg, insufficient different angles of attack were available to fit such a model, and thus the model was changed to 2nd order in angle of attack instead. 95% nonsimultaneous confidence intervals were computed to quantify the accuracy of the response models.

4. Response models propeller performance

Polynomial response models for the propeller performance were generated for the thrust and torque coefficients with respect to angle of attack and advance ratio at fixed pitch using the data from the rotating shaft balance. Quadratic models with full interaction terms were used to fit the thrust and power coefficients C_T and C_P. The other propeller performance parameters were derived from these coefficients in combination with the advance ratio.

III. Experimental Results

A. Effects of Nacelle Installation

Application of a tip-mounted propeller means that a nacelle needs to be installed on the wingtip. This modifies the aerodynamic characteristics of the wing. The nacelle-on, blades-off configuration was used to assess this effect by comparison with the data from the nacelle-off configuration. The results presented in this section were obtained at a freestream Mach number of 0.120. Figure 5 compares the lift and drag performance for the two configurations.

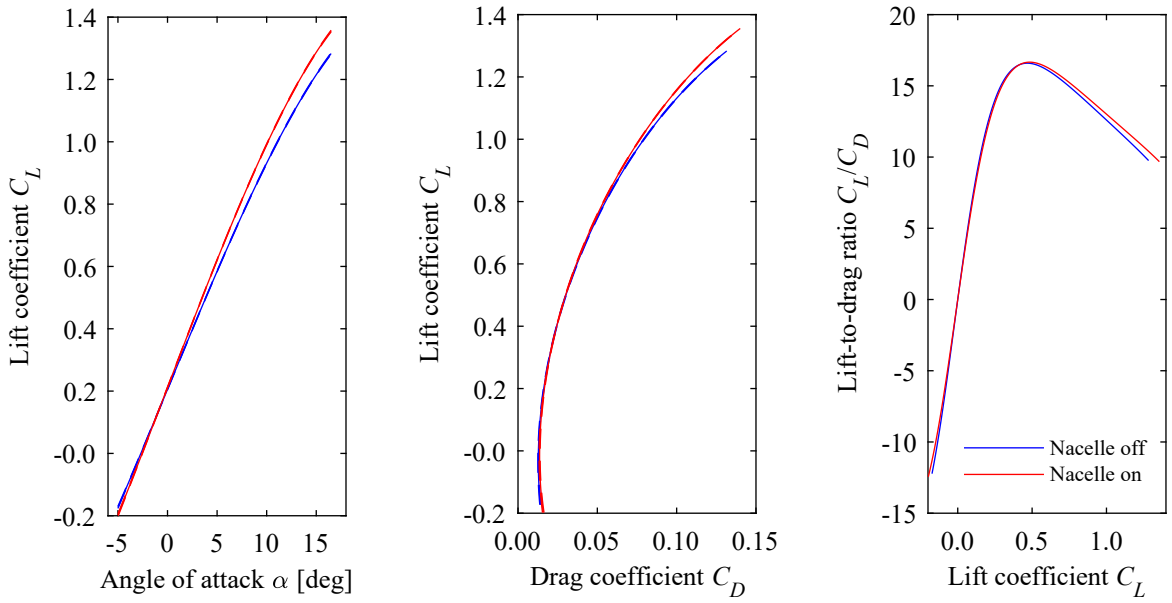

(a) Lift polar **(b) Drag polar** **(c) Lift-to-drag ratio**

Fig. 5 Effect of nacelle installation on system lift and drag. 95% confidence intervals displayed by the dashed lines.

Figure 5 shows that the installation of the nacelle has 3 major impacts:

- Increased wing lift coefficient due to nacelle-induced upwash and a reduction in wing downwash through increased effective aspect ratio.
- Decreased induced drag due to increased effective aspect ratio. This translates into higher lift coefficient at fixed drag coefficient.
- Increased friction drag due to increased wetted area. This translates into higher drag at low lift coefficients.

The lift-to-drag ratio (Fig. 5c) around the design lift coefficient ($C_L = 0.5$) is not much affected by the installation of the nacelle. At this condition, the beneficial effects of the effective aspect-ratio increase are cancelled by the increased friction drag and the nacelle-induced upwash is still small.

The comparison of the nacelle-off and nacelle-on configurations showed the expected phenomena and suggests that the installation of the nacelle on the model did not introduce major undesired aerodynamic phenomena such as separation. Therefore, the nacelle-off configuration was considered as a good baseline for quantification of the propeller effect.

B. Effects of Propeller Thrust Setting

Operation of the propeller modifies the system and wing loads due to the propeller-wing interaction. The raw measurement data were used to define response models for the system and propeller forces. These response models were then used to separate the propeller and wing performance. This enabled an assessment of the propeller effect on the wing aerodynamic efficiency. Both positive and negative thrust settings were considered. All results presented in this section were obtained at a freestream Mach number of 0.120.

1. System performance

The system forces were measured with the external balance. Figures 6 and 7 provide the system lift and drag polars for propeller operation at 45 deg pitch (positive thrust) and 30 deg pitch (negative thrust), respectively. The system drag is expressed in terms of the net streamwise force coefficient C_X, which is defined positive in the negative drag direction (i.e. $C_X > 0$ implies excess thrust). For reference, the performance of the nacelle-on, blades-off configuration is also included in the figures.

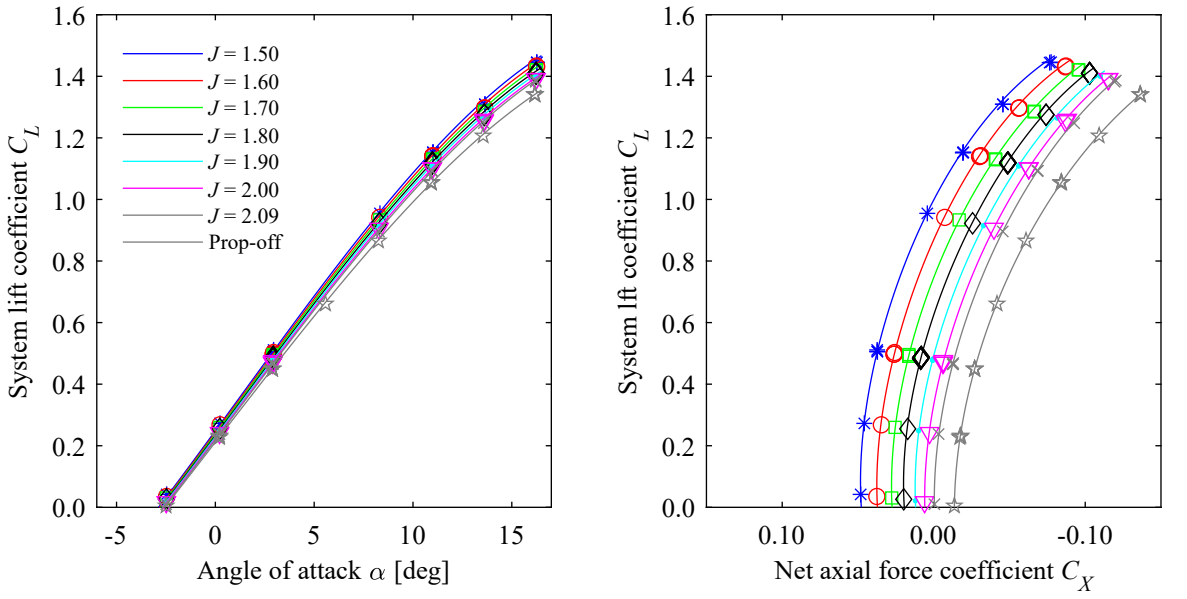

(a) Lift **(b) Drag direction (positive values indicate excess thrust)**

Fig. 6 System forces with propeller enabled; positive thrust, $\beta_{0.7R} = 45$ deg.

The results at positive thrust setting shown in Fig. 6 display the expected performance trends which match with previous findings. Operation of the propeller increases the wing lift due to local enhancement of dynamic pressure and effective angle of attack on the outboard part of the wing. The effect increases in magnitude with increasing thrust coefficient and torque coefficient. In terms of system drag, the slope of the drag polar increases with operation of the propeller. Increasing angle of attack increases thrust in the flight direction, which shows up as a decrease in system drag. Moreover, the propeller effect modifies the wing performance due to the beneficial swirl effect. The net streamwise force coefficient becomes positive when operating the propeller due to the propeller thrust offsetting the wing and nacelle drag. At the highest angles of attack considered, only the lowest advance ratio at 30 deg pitch (not shown here) resulted in sufficient thrust to offset the wing and nacelle drag and achieve a net zero force in the streamwise direction.

When operating the propeller at negative thrust (Fig. 7), the propeller effect decreases system lift. This is due to the reduction in dynamic pressure and effective angle of attack in the area of the wing washed by the slipstream. As a result, the entire configuration would need to be operated at an increased angle of attack to maintain the desired lift coefficient compared to the propeller-off condition. The drag polars still become steeper due to the propeller interaction effect. This is an unexpected result. In order to explain it better, the wing and propeller forces need to be assessed separately. This will be done in the next subsection.

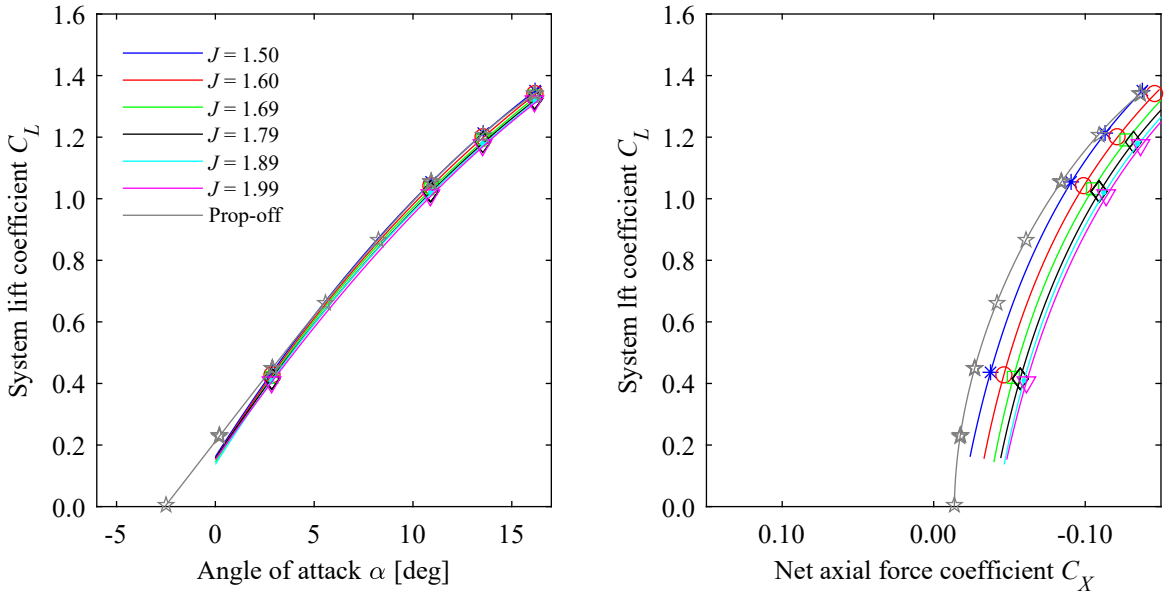

(a) Lift **(b) Drag direction (positive values indicate excess thrust)**

Fig. 7 System forces with propeller enabled; negative thrust, $\beta_{0.7R}$ = 30 deg.

2. Separation between wing and propeller performance

The measurement data from the external balance and rotating balance were combined to enable a separation between the forces/moments created by the wing with nacelle on the one hand, and the propeller on the other hand.

Figure 8 plots the lift-to-drag ratio of the wing, excluding the forces on the rotating part of the setup, as a function of the wing lift coefficient, for propeller pitch settings of $\beta_{0.7R}$ = 45 deg (positive thrust), and $\beta_{0.7R}$ = 30 deg (negative thrust).

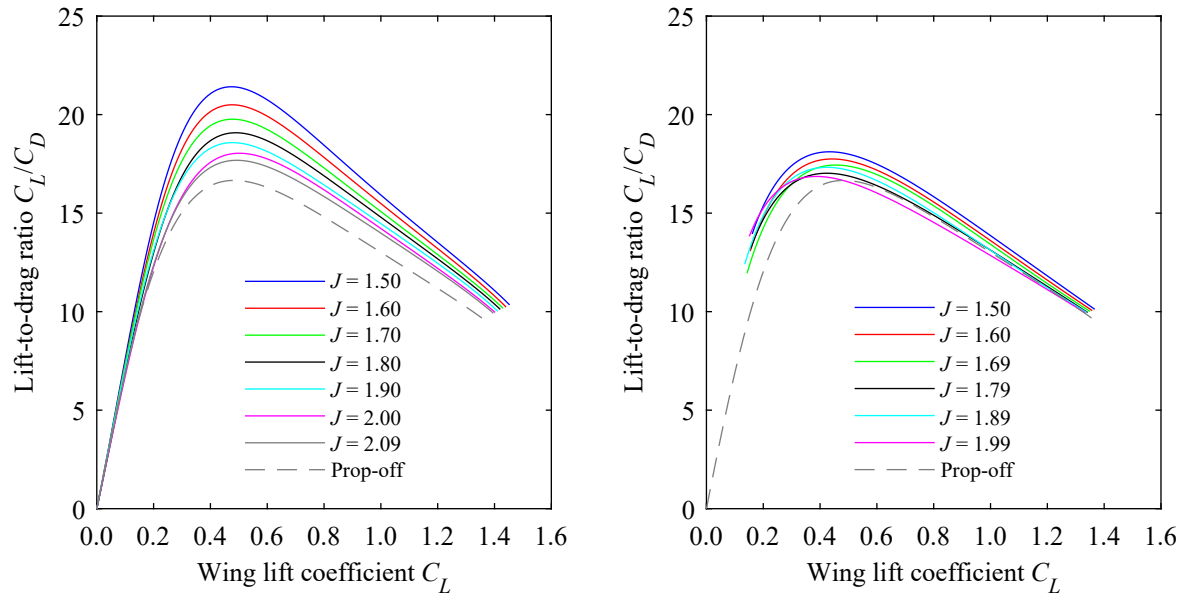

(a) Positive thrust: $\beta_{0.7R}$ = 45 deg **(b) Negative thrust: $\beta_{0.7R}$ = 30 deg**

Fig. 8 Effect of propeller thrust at constant advance ratio on wing aerodynamic performance at constant lift coefficient.

The results shown in Fig. 8 provide evidence of the beneficial interaction effect between propeller and wing for tip-mounted propeller configurations.

At positive thrust (Fig. 8a), the propeller-induced upwash (due to swirl) creates a net reduction in wing drag due to lift and thereby increases the aerodynamic efficiency of the wing. At the highest thrust setting considered ($\beta_{0.7R} = 30$ deg, $J = 0.90$; not shown here), the increase in maximum wing L/D was up to 45%. It should be noted that the propeller thrust at constant advance ratio is not constant with changing wing lift coefficient, and therefore the comparison provided in these figures is not completely fair. This will be solved in the next subsection in which the component performance is compared at constant net streamwise force coefficient.

At negative thrust (Fig. 8b), a reduction in wing performance was expected due to the opposite swirl in the slipstream at this condition. However, the results show that despite the operation at negative thrust, still a noticeable increase in wing aerodynamic efficiency was measured. This suggests that for this model at these operational conditions, the propeller-induced downwash and axial-velocity deficit improved the wing lift distribution compared to the propeller-off case. For simplicity, the wing did not feature any twist. As a result, the baseline propeller-off configuration may not have featured optimal performance. This should be kept in mind when comparing the propeller-off and propeller-on results in terms of aerodynamic efficiency.

Figures 9 and 10 provide the forces on the rotating part of the setup in the installed condition as a function of angle of attack at propeller pitch settings of $\beta_{0.7R} = 45$ deg (positive thrust), and $\beta_{0.7R} = 30$ deg (negative thrust), respectively. The definition of efficiency is different in the positive and negative thrust regimes. At positive thrust, the conventional definition for propeller efficiency is used ($\eta = TV_\infty/P$). At negative thrust, the turbine efficiency is used ($\eta = P/TV_\infty$).

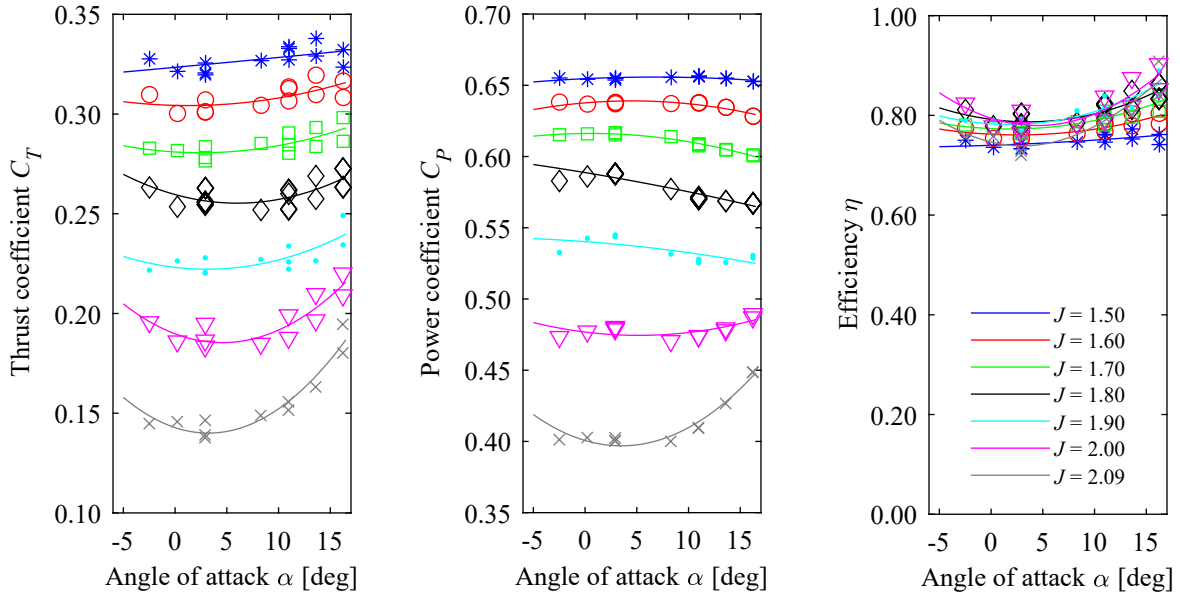

(a) Thrust ($C_T = T/(\rho_\infty n^2 D^4)$) **(b) Power** ($C_P = P/(\rho_\infty n^3 D^5)$) **(c) Efficiency** ($\eta = TV_\infty/P$)

Fig. 9 Propeller loads in installed configuration at constant advance ratio as a function of angle of attack; $\beta_{0.7R} = 45$ deg, positive thrust.

Figure 9 displays the expected results for the configurations at positive thrust. The propeller thrust and power coefficient (defined in propeller reference frame, along the propeller axis) increase with increasing angle of attack. This is because the increase in effective dynamic pressure and angle of attack at the downgoing blade section have a larger combined effect than the reduction in effective dynamic pressure and angle of attack on the upgoing blade side. This is well known from literature. The propeller thrust coefficient increases more rapidly than the power coefficient, leading to an increase in propeller efficiency. When defining the efficiency with respect to the thrust produced in the flight direction (not aligned with the propeller axis), the efficiency benefit decreases at low thrust settings, while at high angle of attack and low advance ratio the efficiency even decreases slightly.

Figure 10 shows that in the negative thrust regime, the propeller thrust and power become less negative upon increasing the angle of attack. This is because of the same mechanism as in the positive thrust mode. The thrust

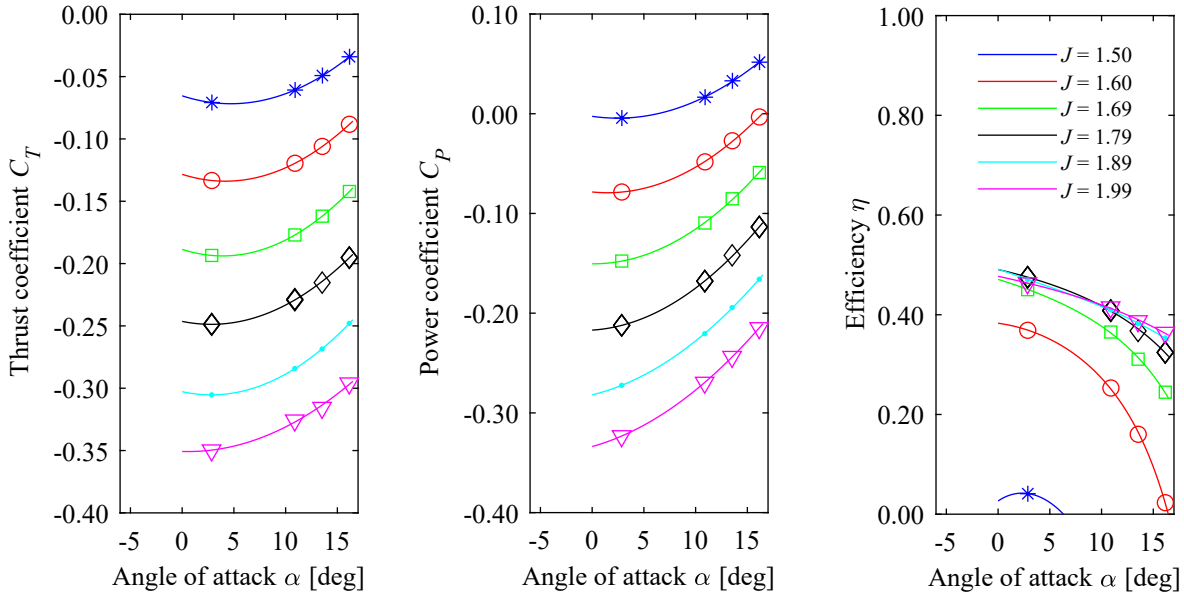

(a) Thrust ($C_T = T/(\rho_\infty n^2 D^4)$) **(b) Power** ($C_P = P/(\rho_\infty n^3 D^5)$) **(c) Efficiency** ($\eta = P/TV_\infty$)

Fig. 10 Propeller loads in installed configuration at constant advance ratio as a function of angle of attack; $\beta_{0.7R} = 30$ deg, negative thrust.

coefficient still increases (i.e. becomes less negative) than the power coefficient. As a result, the efficiency in this regime decreases with increasing angle of attack, because it is defined in a reversed way compared to the propulsive mode (shaft power over drag power as opposed to thrust power over shaft power). Moreover, the reduction in negative thrust coefficient means that the braking capability of the propeller decreases with increasing angle of attack.

3. Wing and propeller performance at constant streamwise force coefficient

The previous results compared wing and propeller performance at fixed advance ratio and varying angle of attack. However, when changing the angle of attack, the wing lift and drag change but also the propeller thrust and torque. Therefore, the assessment of the effects of the interactions in this way is not insightful to draw conclusions about performance at system level. Instead, the wing and propeller performance was extracted at constant system lift coefficient and net streamwise force coefficient.

Positive net streamwise force ($C_X = +0.06$)

The positive thrust case was assessed at a positive net streamwise force coefficient of $C_X = +0.06$. This indicates an excess thrust of about 2 times the wing drag at a design lift coefficient of $C_L = 0.5$. The representativeness of this net streamwise force coefficient depends on the aircraft design, thrust split between tip-mounted propellers and potential main (inboard) propellers, and mission profile. Figure 11 provides the separation between propeller and wing force coefficients at this condition. The corresponding operational conditions are provided in Fig. 12. For comparison reasons, this figure also includes the conditions required to achieve different net streamwise force coefficients ($C_X = 0.00, +0.04, +0.08$).

The results shown in Fig. 11 confirm the hypothesis that the impact of the propeller installation effects grows with increasing propeller thrust setting. Compared to the results at a net streamwise force coefficient of $C_X = 0.00$ (not presented here), the results at $C_X = +0.06$ show higher changes between the propeller-off and propeller-on data. The increased axial velocity in the propeller slipstream leads to a larger increase in lift coefficient at a given angle of attack. The increased swirl leads to an increased beneficial effect on wing lift-to-drag ratio. At the design lift coefficient of $C_L = 0.5$ the increase is 31%. This relative increase in wing lift-to-drag ratio remains approximately constant with increasing wing lift coefficient. At $C_L = 1.0$, which matches better with the excess thrust scenario considered here, the increase in lift-to-drag ratio compared to the unpowered configuration was 32%.

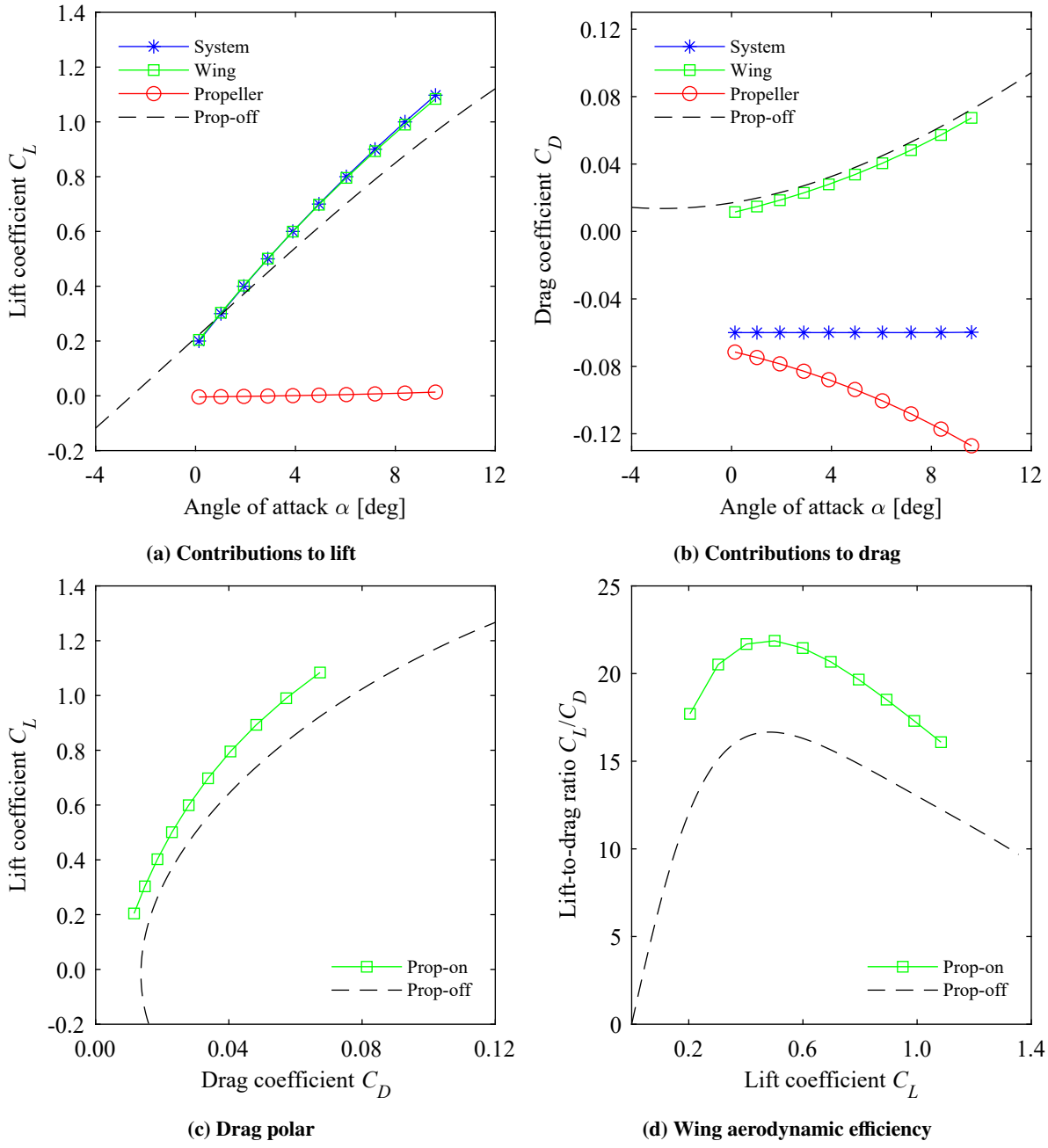

(a) Contributions to lift

(b) Contributions to drag

(c) Drag polar

(d) Wing aerodynamic efficiency

Fig. 11 Propeller effect on component performance; $C_X = +0.06$**,** $\beta_{0.7R} = 30$ **deg.**

The operating conditions plotted in Fig. 12 match the trends observed for the case with zero net streamwise force (not presented here) and follow the expected trends. The higher the net positive streamwise force or lift coefficient required, the higher the propeller thrust setting. This then translates in higher power consumption as well. The propeller efficiency remains reasonably similar between the different cases at positive net streamwise force coefficient. This suggests that the selected pitch setting was appropriate. For the real aircraft, the changes in efficiency between the different cases would be even smaller because the propeller would feature variable pitch and thus a flatter efficiency response.

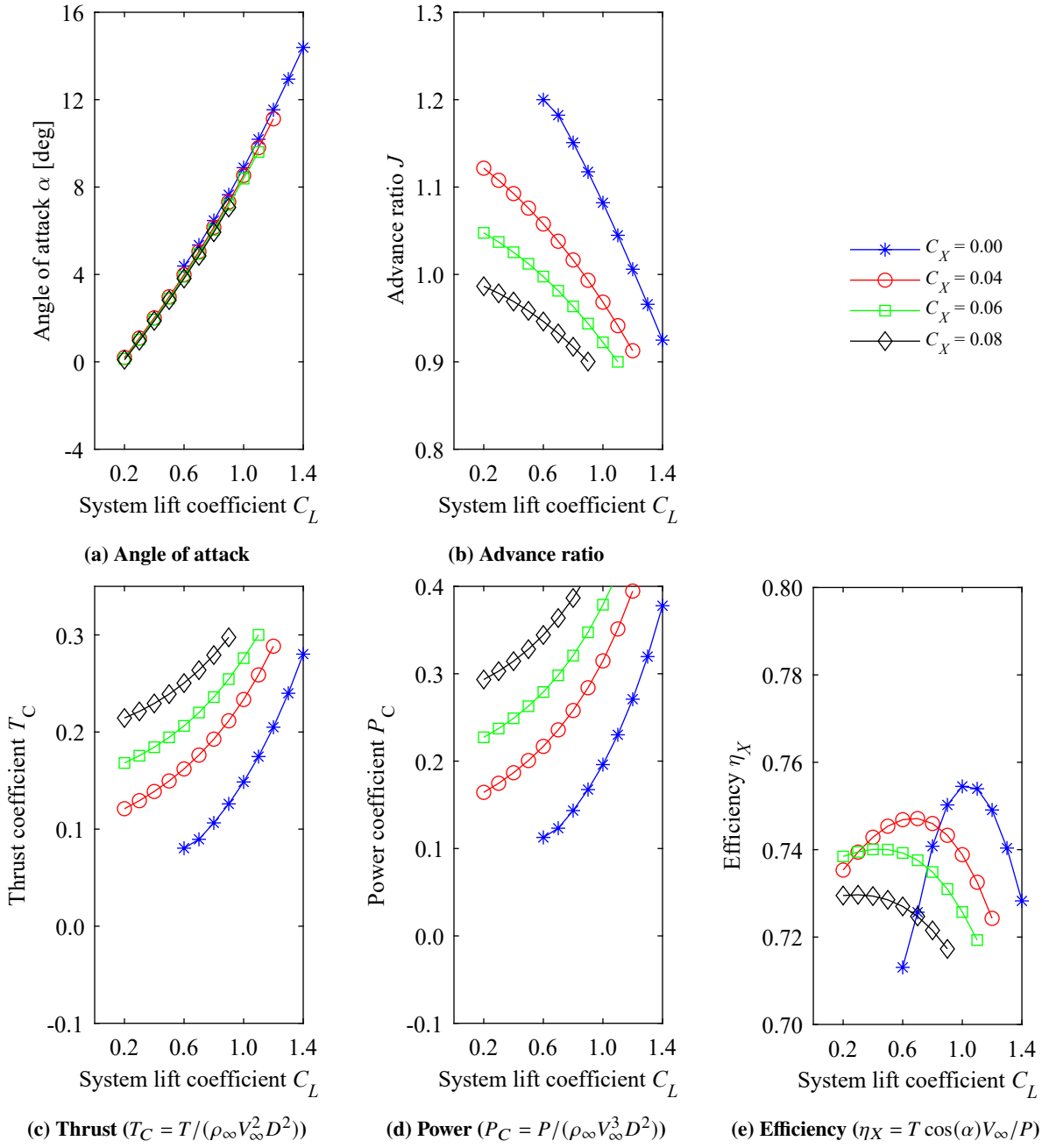

(a) Angle of attack **(b) Advance ratio**

(c) Thrust ($T_C = T/(\rho_\infty V_\infty^2 D^2)$) **(d) Power** ($P_C = P/(\rho_\infty V_\infty^3 D^2)$) **(e) Efficiency** ($\eta_X = T\cos(\alpha)V_\infty/P$)

Fig. 12 System and propeller settings to reach different positive net streamwise force coefficients at different lift coefficients, $\beta_{0.7R} = 30$ deg.

Negative net streamwise force ($C_X = -0.06$)

For the negative thrust regime, it was expected that the reduction in dynamic pressure and adverse propeller-induced downwash in the slipstream would lead to a reduction in wing performance compared to the propeller-off case. To test this hypothesis, data were also extracted at a net negative streamwise force coefficient. For this analysis, a value of $C_X = -0.06$ was selected, which indicates an excess drag of about 2 times the wing drag at a design lift coefficient of $C_L = 0.5$. This is the opposite of the positive excess thrust considered in the previous subsection. Figure 13 displays the model performance in terms of system, wing, and propeller lift and drag/thrust at this condition. The corresponding operational conditions are provided in Fig. 14. For comparison reasons, this figure also includes the conditions required to achieve different net streamwise force coefficients ($C_X = 0.00, -0.04, -0.08$).

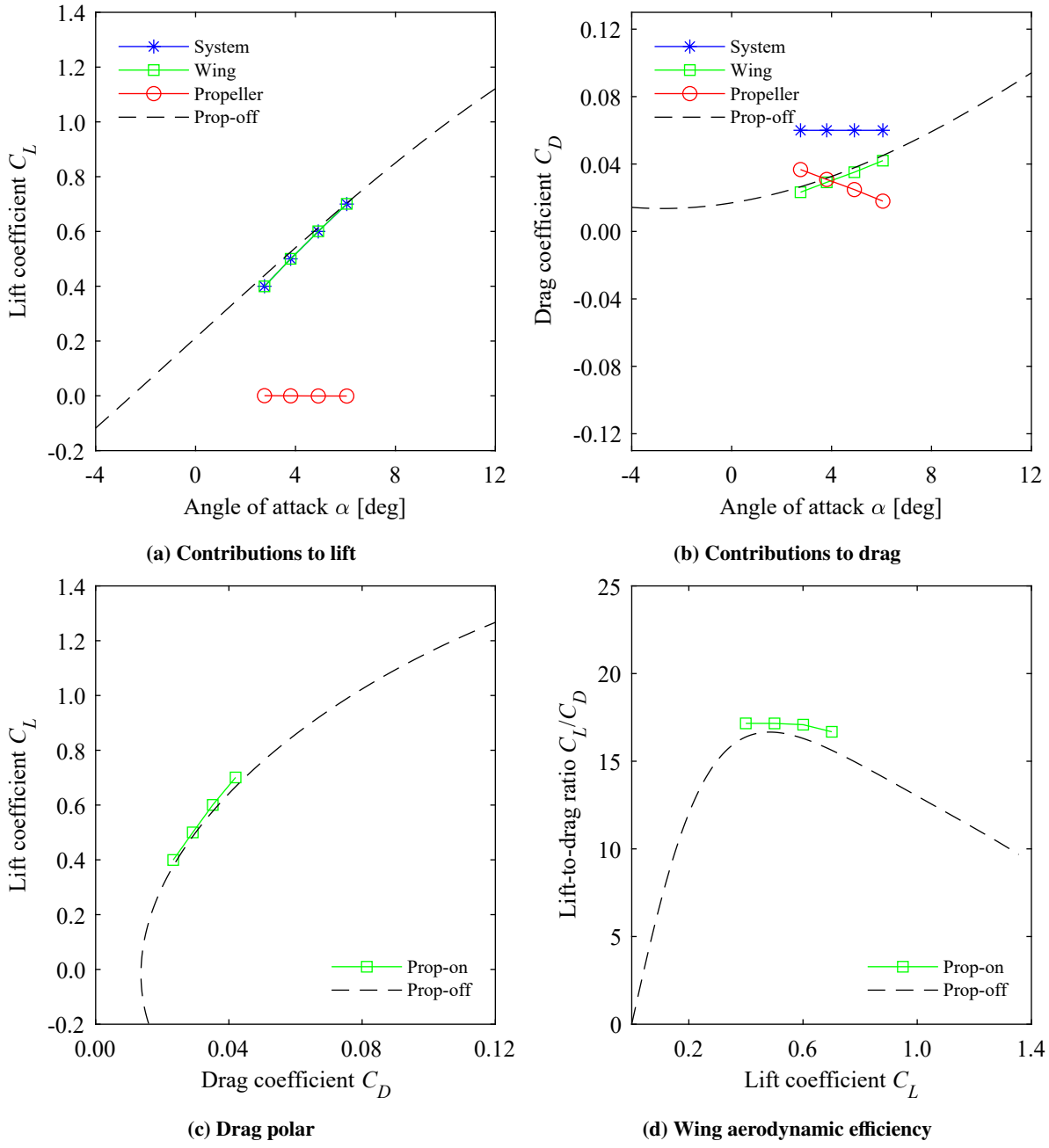

(a) Contributions to lift

(b) Contributions to drag

(c) Drag polar

(d) Wing aerodynamic efficiency

Fig. 13 Propeller effect on component performance; $C_X = -0.06$, $\beta_{0.7R} = 30$ deg.

The results of Fig. 13 suggest that the hypothesis that the operation at negative propeller thrust would worsen the wing performance can be partially rejected.

Figure 13a shows that the wing lift coefficient does decrease at negative thrust setting compared to the case without propeller. This is due to a combination of the reduced dynamic pressure and downwash experienced by the part of the wing immersed in the propeller slipstream when operating at negative thrust setting.

Considering the wing drag, on the other hand, it can be seen in Fig. 13b that at a given angle of attack, the installed wing drag was lower than that of the propeller-off configuration. Figure 13c shows that at fixed lift coefficient the installed wing drag was also lower than that of the propeller-off configuration. This can be due to two different effects. First, the reduced dynamic pressure in the propeller slipstream induces a reduction in friction drag on the part of the wing immersed in the slipstream. Second, the propeller-induced downwash may improve the wing lift distribution in

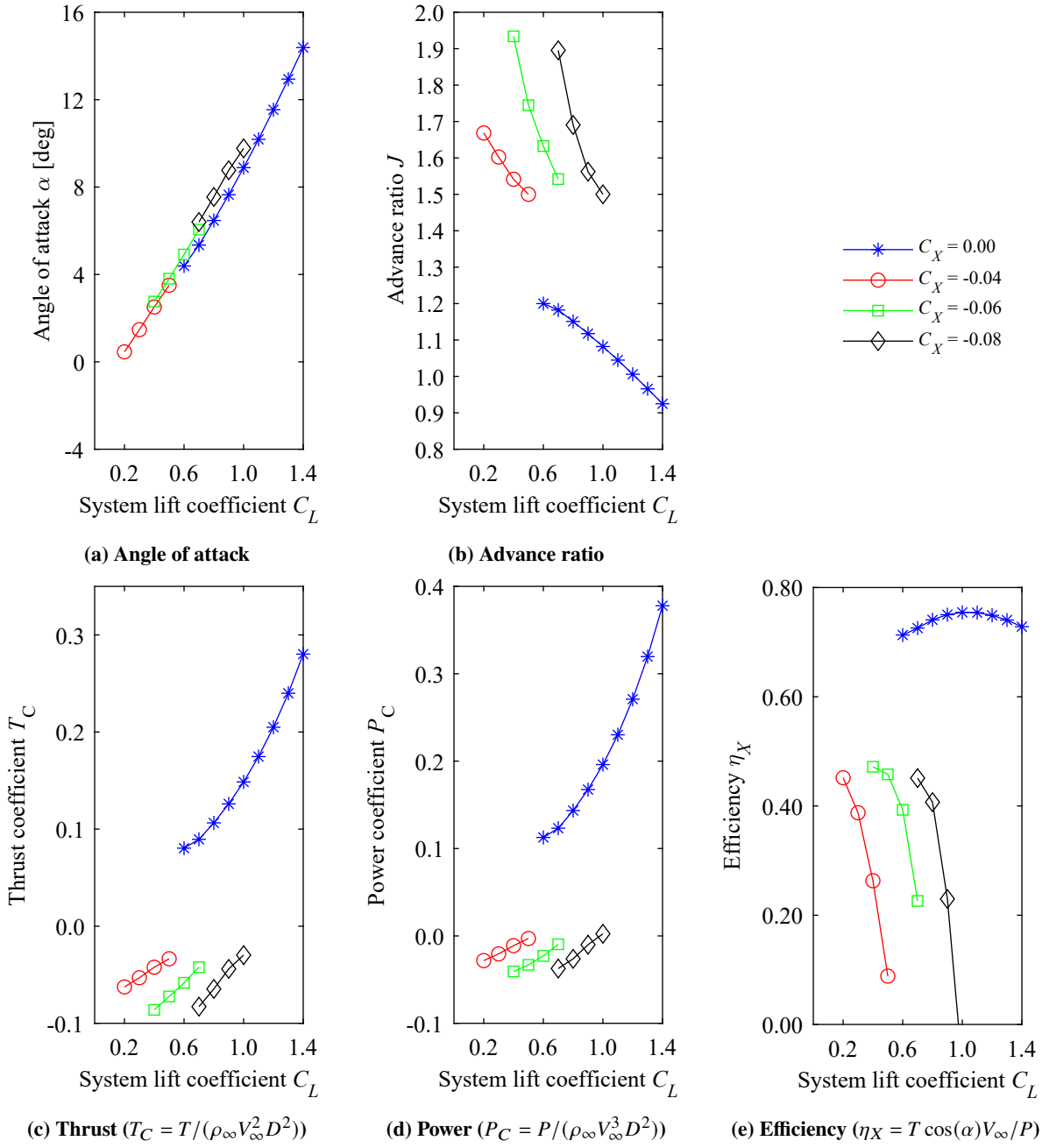

(a) Angle of attack **(b) Advance ratio**

(c) Thrust ($T_C = T/(\rho_\infty V_\infty^2 D^2)$) **(d) Power** ($P_C = P/(\rho_\infty V_\infty^3 D^2)$) **(e) Efficiency** ($\eta_X = T\cos(\alpha)V_\infty/P$)

Fig. 14 System and propeller settings to reach different negative net streamwise force coefficients at different lift coefficients, $\beta_{0.7R} = 30$ deg.

case the lift distribution for the propeller-off case was not optimal. This is possible considering the lack of wing twist in the design. This would not be the case for a real configuration for which the wing would have been optimized for best performance in the absence of the propeller. It is not expected that the minor shift in angle of attack required to reach a given lift coefficient is responsible for the observed performance increase for the prop-on configurations. This is because the lift-to-drag ratio curve remains above that of the propeller-off case over a wide range of lift coefficients.

Due to the limited negative thrust range considered during the experiment (Fig. 14c), trimmed conditions at a specific net streamwise force coefficient could only be achieved for a limited range of lift coefficients. Additional pitch settings should be considered in future experiments to widen this range.

The results of Fig. 14 show that the power output from the propeller is largely constrained by the acceptable drag generated by the propeller. With increasing lift coefficient, the wing drag increases and thus the acceptable amount of negative thrust from the propeller to achieve a net streamwise force coefficient decreases. This imposes a bound on the power extraction from the flow because lower negative thrust in principle means lower power output from the propeller.

Wing lift-to-drag ratio versus net streamwise force coefficient

To summarize the propeller effect on the wing lift-to-drag ratio, Fig. 15 displays the change in wing lift-to-drag ratio curves with net streamwise force coefficient. Both positive and negative thrust settings are included, as well as the baseline propeller-off configuration. It can be seen that at positive thrust settings, the wing lift-to-drag ratio increases with increasing thrust setting, over the entire range of lift coefficients considered. All cases at negative thrust setting also show increased wing lift-to-drag ratio though compared to the propeller-off condition. This shows that even at negative thrust setting, the wing performance can benefit from propeller installation effects. It should be investigated further to what extent this can be explained by a suboptimal wing design (e.g. zero twist).

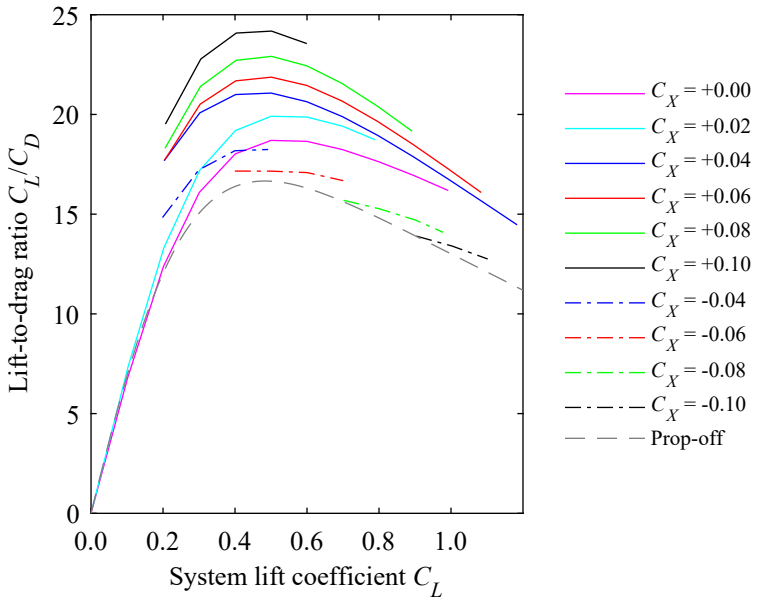

Fig. 15 Wing lift-to-drag ratio for different values of net streamwise force coefficient.

C. Effects of propeller on aileron effectiveness

Because of the proximity of the tip-mounted propeller to the aileron, it was expected that the operation of the propeller would have a significant impact on the aileron performance, and thus roll-control capabilities of the aircraft. To study this, measurements were taken with the aileron deflected at 0, +10 and −10 degrees for the nacelle-on configuration with propeller blades on and off.

The goal of the aileron is to provide roll control. Figure 16 displays the rolling moment coefficient as a function of angle of attack for the three aileron settings considered for the propeller-off, positive thrust ($\beta_{0.7R}$ = 45 deg), and negative thrust ($\beta_{0.7R}$ = 30 deg) configurations. Note that the model was a half model, so the rolling moment observed here is a direct effect of the spanwise lift distribution. For the negative thrust case unfortunately no results were available at the negative aileron deflection setting.

The results for the propeller-off configuration (Fig. 16a) show that the rolling moment increases approximately linearly with angle of attack, suggesting that the amplitude of the lift distribution scales approximately linearly with angle of attack without major shifts in the spanwise distribution. The deflection of the aileron modifies the lift on the outboard part of the wing, thereby modifying the rolling moment coefficient. At positive aileron deflection, the lift on the outboard part of the wing increases, thus increasing the rolling moment coefficient. For the negative aileron deflection, the opposite occurs. Again, approximately linear responses are observed for all aileron deflection angles, suggesting that the considered cases are appropriate for further analysis of the propeller effect on the aileron effectiveness.

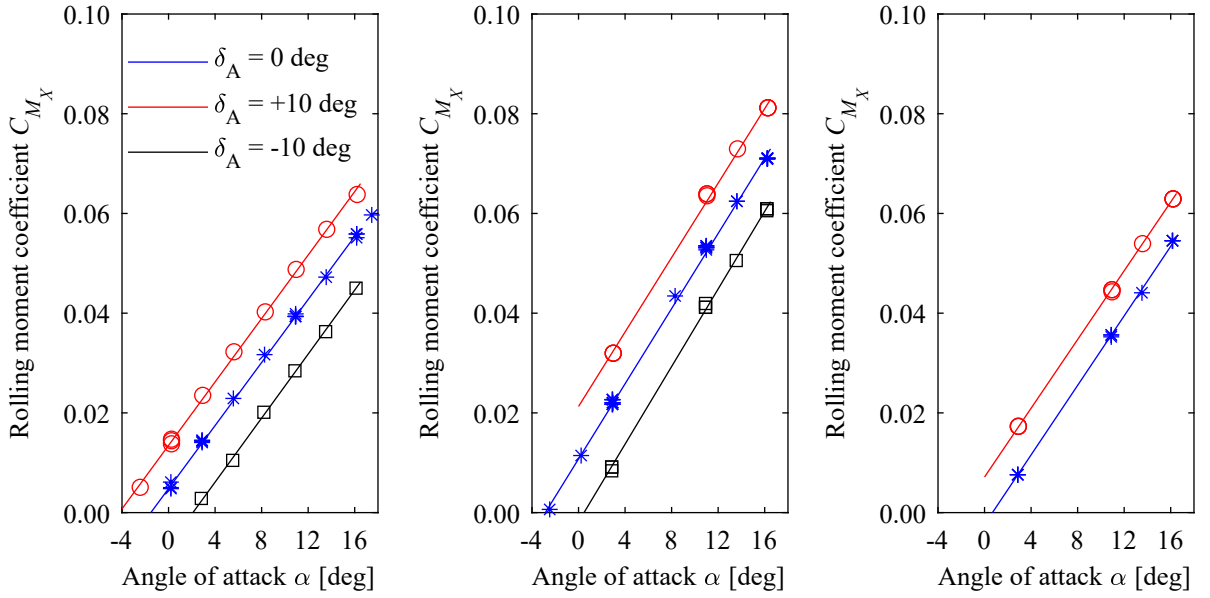

(a) Propeller-off **(b) Pos. thrust:** $\beta_{0.7R}$ = 45 **deg,** J = 1.8 **(c) Neg. thrust:** $\beta_{0.7R}$ = 30 **deg,** J = 1.8

Fig. 16 Effect of aileron deflection angle on rolling-moment coefficient at different angles of attack.

The propeller-on results of Figs. 16b and 16c suggest that also with the propeller on the effects of the aileron deflection are sufficiently linear to assess aileron effectiveness with a simple linear model. This was done to assess the impact of propeller operation on the aileron effectiveness. Forward differencing was applied on the available data to compute the gradient of rolling moment coefficient to aileron deflection angle.

The results are shown in Fig. 17, which compares three cases: operation at positive thrust ($\beta_{0.7R}$ = 45 deg, J = 1.8), operation at negative thrust ($\beta_{0.7R}$ = 30 deg, J = 1.8), and the propeller-off baseline.

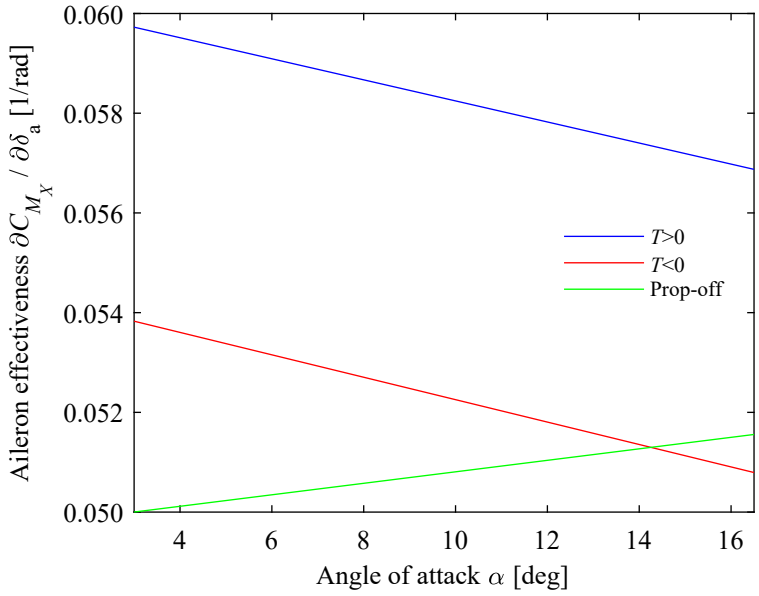

Fig. 17 Effect of propeller operation at positive and negative thrust on aileron effectiveness.

Figure 17 shows that the operation of the propeller at positive thrust increases the aileron effectiveness. This will be due to a combination of the increased lift gradient on the outboard part of the wing due to the increased dynamic

pressure there, and possibly a change in propeller-induced forces with aileron setting that also contribute to the change in rolling moment. These need to be investigated separately in future work. Operation at negative thrust decreases the aileron effectiveness by about 10% compared to the positive thrust case. This is a direct effect of the dynamic pressure reduction in the slipstream when operating the propeller at negative thrust. However, even at negative thrust setting the aileron effectiveness with propeller enabled is still higher than that of the propeller-off baseline for angles of attack below angles of attack of approximately 14 degrees. This suggests that operation at negative thrust is not critical for aileron performance. Apparently, the propeller-induced pressure gradient does not promote separation on the outboard wing, or this is sufficiently opposed by the propeller-induced downwash. However, this could still represent a design issue if the ailerons are to be sized for asymmetric stall at low-speed high angle-of-attack conditions.

D. Propeller-wing wake flowfields

Wake survey measurements were performed with a rake of 5-hole Pitot probes to analyze the flow downstream of the model. The study of the flow properties and topology in the wake of the model allows for a deeper understanding of the main flow phenomena occurring in the flowfield around the model. Figure 18 shows the total pressure distribution in the wake survey plane for propeller-off and -on configurations. In particular, the total pressure coefficient is shown, defined as $C_{p_t} = (p_t - p_{t_\infty})/q_\infty$. For the propeller-on cases, both positive and negative thrust conditions were studied. The test conditions correspond to $J = 1.80$ at $\beta_{0.7R} = 45$ deg and $\beta_{0.7R} = 30$ deg for the positive and negative thrust regimes, respectively. The measurements were carried out at a wing (uncorrected) angle of attack of 10 deg, corresponding to a (clean) wing lift coefficient of around 1.0.

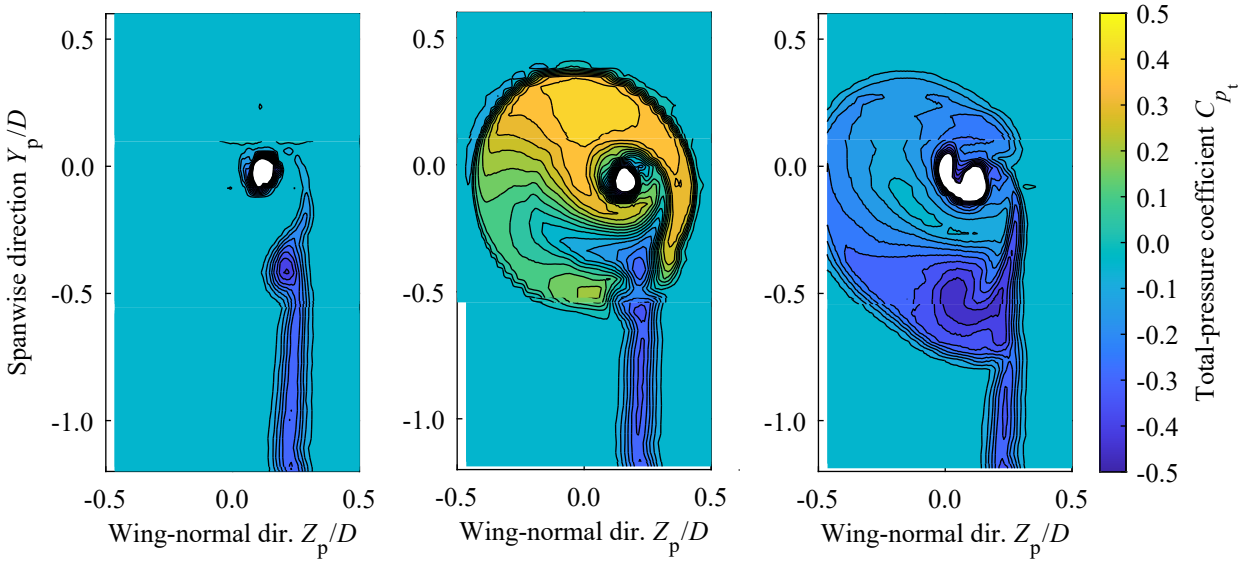

(a) Propeller-off **(b) Pos. thrust: $\beta_{0.7R} = 45$ deg** **(c) Neg. thrust: $\beta_{0.7R} = 30$ deg**

Fig. 18 Total-pressure distribution in the wake of the model; $\alpha = 10$ deg, $\delta_a = 0$ deg, $J = 1.8$, $M_\infty = 0.12$. (Propeller rotation is clockwise).

In the propeller-off case of Fig. 18a the viscous wake of the wing and of the nacelle are clearly shown. The low total pressure found in the wing wake is due to the viscous dissipation occurring in the boundary layer of the wing. Moreover, around the nacelle the flow is deformed due to the lift and tip-vortex roll-up. Finally, the presence of a low-momentum region at the outer edge of the aileron can be noted, albeit at $\delta_a = 0$ deg. This might be due to the presence of a gap between the aileron and the fixed wing parts, which induces a drop in the local lift and hence shed vorticity and higher dissipation.

When the propeller is operating at positive thrust setting (Fig. 18b), the propeller slipstream is characterized by a total pressure that is higher than the freestream. This is due to the momentum increase in the flow introduced by the propeller (directly related to the propeller thrust). Since the propeller operates at an incidence angle and due to the

interaction with the wing flow, the propeller slipstream appears distorted and non-uniform. In particular, the slipstream entrains low-momentum flow from the wing wake as a consequence of the swirl induced by the propeller.

At negative thrust setting (see Fig. 18c), the propeller slipstream shows a negative total pressure coefficient. This is a consequence of the decrease in momentum across the propeller which results in a negative propeller thrust. In this regime, the propeller reduces the dynamic pressure and effective angle of attack perceived by the wing tip. As a consequence, the junction flow between the wing and nacelle is affected, resulting in a stronger total pressure deficit in the inboard part of the wing tip.

IV. Conclusions

A wind-tunnel experiment was performed at the DNW Low-Speed Tunnel with a powered propeller-wing model. A tip-mounted propeller configuration was simulated, with the propeller operating at positive and negative thrust settings. Analysis of the results led to the following conclusions:

- Installation of a nacelle at the tip of a wing increases the lift gradient and decreases induced drag. However, this drag benefit is largely offset by an increase in viscous drag, thereby leading to a net similar aerodynamic efficiency for both configurations. Design optimization would be required to optimize the nacelle-wing integration.
- At positive thrust setting, the increased dynamic pressure and upwash induced by the propeller lead to an increase in wing lift gradient and thus lift coefficient at a fixed angle of attack. Furthermore, the induced drag of the system decreases due to the beneficial swirl effect. This drag reduction is much larger than the increase in friction drag, thereby leading to a net increase in wing aerodynamic efficiency at fixed lift and net streamwise force coefficients. In cruise-like conditions, $C_L = 0.5$ and $C_X = 0.00$ (not presented in the paper), the increase in wing lift-to-drag ratio was 12%. In climb-like conditions, $C_L = 1.0$ and $C_X = 0.06$, the increase in wing lift-to-drag ratio was 32%. The precise benefit of the tip-mounted propeller depends on the details of the geometry, thrust share of the tip-mounted propellers, and baseline wing design.
- At negative thrust setting, the decreased dynamic pressure and downwash induced by the propeller lead to a decrease in wing lift gradient and thus lift coefficient at a fixed angle of attack. However, the wing lift-to-drag ratio was found to still improve compared to the propeller-off condition. This could be due to two different mechanisms: the reduced dynamic pressure in the propeller slipstream induces a reduction in friction drag on the part of the wing immersed in the slipstream, and the propeller-induced downwash may improve the wing lift distribution in case the lift distribution for the propeller-off case was not optimal.
- Operation at negative thrust decreases the aileron effectiveness by about 10% compared to the positive thrust case. This is a direct effect of the dynamic pressure reduction in the slipstream when operating the propeller at negative thrust. However, even at negative thrust setting the aileron effectiveness with propeller enabled is still higher than that of the propeller-off baseline for angles of attack below approximately 14 degrees and therefore it is concluded that operation at negative thrust is not critical for aileron performance.
- Operation at negative thrust leads to an expansion of the slipstream downstream of the propeller. Compared to the positive thrust case, this increases the amount of wing area exposed to the modified flow properties in the slipstream. Moreover, the total pressure in the slipstream is decreased instead of increased. Also, the junction flow between the wing and nacelle is affected, resulting in a stronger total pressure deficit in the inboard part of the wing tip than for the positive thrust case.

The experiment has resulted in a rich dataset which will be prepared for sharing with the community. Once available, the dataset will serve as a unique validation case for benchmarking of numerical tools.

Acknowledgments

The research leading to these results has received funding from the European Union's Horizon 2020 Research and Innovation programme under Grant Agreement No 875551. This publication is part of the project 'Regenerative propellers: sustainable and quiet electric propeller aircraft with in-flight energy recovery' with project number 19082 of the research programme NWO-Talent Program Veni AES 2021 which is (partly) financed by the Dutch Research Council (NWO).

Funded by the European Union

NWO

The authors would like to thank Stephan van 't Hof, Lars Leenheer, Ed Roessen, Peter den Dulk, Rob van der List, and Frank Schilder from Delft University of Technology's electronic and mechanical support division (DEMO) for their contributions to the design and manufacturing of the model and electronic equipment. Furthermore, the technical

support during the test campaign of Martijn van Sluis, Robert Nederlof, Ramon Duivenvoorden, and Nando van Arnhem was greatly appreciated. Finally, we would like to thank the colleagues at DNW, in particular Iwan Philipsen, Mia Jovetić, Wouter Noort, Alfons Brinkhuis, and Gerrit Feenstra for their support in the preparation and execution of the test campaign.

References

[1] Snyder, M. H., Jr., and Zumwalt, G. W., "Effects of Wingtip-Mounted Propellers on Wing Lift and Induced Drag," *Journal of Aircraft*, Vol. 6, No. 5, 1969, pp. 392–397. https://doi.org/10.2514/3.44076.

[2] Miranda, L. R., and Brennan, J. E., "Aerodynamic Effects of Wingtip-Mounted Propellers and Turbines," *4th Applied Aerodynamics Conference*, AIAA Paper 1986-1802, June 1986. https://doi.org/10.2514/6.1986-1802.

[3] Veldhuis, L. L. M., "Propeller Wing Aerodynamic Interference," Ph.D. thesis, Faculty of Aerospace Engineering, Delft University of Technology, Delft, The Netherlands, 2005.

[4] Sinnige, T., van Arnhem, N., Stokkermans, T. C. A., Eitelberg, G., and Veldhuis, L. L. M., "Wingtip-Mounted Propellers: Aerodynamic Analysis of Interaction Effets and Comparison with Conventional Layout," *Journal of Aircraft*, Vol. 56, No. 1, 2019, pp. 295–312. https://doi.org/10.2514/1.C034978.

[5] Sinnige, T., Nederlof, R., and van Arnhem, N., "Aerodynamic Performance of Wingtip-Mounted Propellers in Tractor and Pusher Configuration," *AIAA AVIATION 2021 Forum*, AIAA Paper 2021-2511, August 2021. https://doi.org/10.2514/6.2021-2511.

[6] McGhee, R. J., Beasley, W. D., and Whitcomb, R. T., "NASA Low- and Medium-Speed Airfoil Development," NASA TM-78709, 1979.

[7] Wentz, W., Seetharam, H., and Fiscko, K., "Force and pressure tests of the GA (W)-1 airfoil with a 20% aileron and pressure tests with a 30% Fowler flap," NASA CR-2833, 1977.

[8] Nahuis, R., and Sinnige, T., "Design, manufacture and commissioning of a new NLR 6-component rotating shaft balance for Delft University of Technology," *10th International Symposium on Strain-Gauge Balances*, Mianyang, China, May 2016.